
Article:
Araújo, T., Parnell, A.J. orcid.org/0000-0001-8606-8644, Bernardo, G. et al. (1 more author) (2023) Cellulose-based carbon membranes for gas separations - unraveling structural parameters and surface chemistry for superior separation performance. Carbon, 204. pp. 398-410. ISSN 0008-6223

https://doi.org/10.1016/j.carbon.2022.12.062

Carbon 204 (2023) 398–410

Contents lists available at ScienceDirect

Carbon

journal homepage: www.elsevier.com/locate/carbon

Cellulose-based carbon membranes for gas separations - Unraveling structural parameters and surface chemistry for superior separation performance

Tiago Araújo [a,b], Andrew J. Parnell [c], Gabriel Bernardo [a,b], Adélio Mendes [a,b,*]

[a] LEPABE - Laboratory for Process Engineering, Environment, Biotechnology and Energy, Faculty of Engineering, University of Porto, Rua Dr. Roberto Frias, 4200-465, Porto, Portugal
[b] ALiCE - Associate Laboratory in Chemical Engineering, Faculty of Engineering, University of Porto, Rua Dr. Roberto Frias, 4200-465, Porto, Portugal
[c] Department of Physics and Astronomy, University of Sheffield, S3 7RH, UK

ARTICLE INFO

Keywords:
Cellulose
Carbon molecular sieve membranes
Urea
SAXS
Gas separation

ABSTRACT

Carbon molecular sieve membranes were prepared from the carbonization of a cellulose-based polymeric precursor doped with urea. The addition of urea to the cellulose precursor induces an increase in structural disorder and an increase in pore volume inside the structure of prepared membranes. This unique preparation procedure proved to be an extremely effective method for tuning the pore size of carbon membranes to the desired separations. Urea acts as a pore-forming agent that allows the fabrication of carbon membranes with high porosity. The addition of 2.8 wt% of urea doubled the permeability of the prepared carbon membrane to hydrogen. In addition, a permeability to oxygen of 333 barrer was obtained, without impairing the selectivity. The proposed preparation procedure is compatible with industrial production and scaling, hopefully making carbon membranes a viable solution to produce oxygen-enriched air, recovering of hydrogen from hydrocarbon streams and carbon dioxide removal from natural gas/biogas.

1. Introduction

The hastening of climate change and global warming caused by the greenhouse gas emissions to the atmosphere is a pressing issue for our society. The anthropogenic nature of this problem requires the development of new technological solutions to achieve the carbon neutrality goals implemented by the European Union for 2050 [1].

Hydrogen or biomethane are considered relevant vectors for this technological transition in the energy, transport and industrial systems [2]. However, the production of these gases requires the removal of CO_2 [3,4]: Moreover, oxygen enriched air–streams allow to increase the efficiency of combustion processes [5]. The oxy-combustion process can reduce the flue gas heat losses, achieving lower emission levels of hydrocarbons, NOx and CO, improving the thermal stability and increasing the productivity [6,7]. In the combustion of natural gas, assuming a temperature of 1500 °C, if an oxygen enriched air stream with only 45% of oxygen is fed to the combustion chamber, a reduction of *ca.* 55% of the natural gas consumption is observed [6,7]; similar trends can certainly be found for coal-fired and biomass power plants [8,9].

Compared with the conventional separation technologies for CO_2 capture, air enrichment or H_2 recovery, such as cryogenic distillation, chemical adsorption or pressure-swing absorption (PSA), membrane separation technologies are the most energy efficient, versatile, low capital cost and environmentally friendly [4,10–12]. Several membrane materials have been developed for gas separations, namely polymeric [13] and inorganic membranes, such as carbon molecular sieves [14–17], metal-organic frameworks (MOFs) [18], zeolite imidazolate framework (ZIF) [19] and graphene oxides [20], among others. Carbon molecular sieve membranes (CMSM) are the most promising alternative not only because their better trade-off between permeability and selectivity but also because their robustness: they are stable even under extremely harsh chemical environments, operating easily under high-pressure and high-temperature applications [4,21,22]. CMSMs display a rigid pore structure with a bimodal pore size distribution: micropores (<2 nm) provide the sorption sites and the ultramicropores (<0.7 nm) enable the molecular sieving mechanism [23]. This pore

* Corresponding author. LEPABE - Laboratory for Process Engineering, Environment, Biotechnology and Energy, Faculty of Engineering, University of Porto, Rua Dr. Roberto Frias, 4200-465, Porto, Portugal.
E-mail address: mendes@fe.up.pt (A. Mendes).

https://doi.org/10.1016/j.carbon.2022.12.062
Received 21 October 2022; Received in revised form 19 December 2022; Accepted 21 December 2022
Available online 23 December 2022

structure, when tuned properly for the desired separation, is responsible for the membrane's high permeability and selectivity [4].

CMSMs are fabricated by the controlled carbonization of a polymeric precursor [24,25]. A correct selection of polymeric precursor is crucial to obtain the desired pore structure and achieve high separation performances [4,21]. Cellulose was the first polymeric precursor used to produce CMSMs and has been one of the most investigated together with polyimides [24–27]. Cellulose is an abundant, renewable and low-cost biopolymer, which makes the development of these membranes more attractive [21]. In addition, cellulose-based CMSMs were the first reported to withstand permeate steams with a relative humidity close to 100% without suffering pore blockage, even at room temperature. This is due to their high hydrophilicity that allows water vapor to permeate the membrane [28,29].

The carbonization conditions of the CMSMs (*i.e.* the carbonization atmosphere and temperature, the heating rate and the soak time) determine the final pore structure and consequently the separation performance of the membranes [30]. By changing these parameters, especially by increasing the final carbonization temperature, it is possible to prepare CMSMs with tighter network of pores making these membranes more selective though less permeable [31]. Regarding cellulose-based CMSMs, Campo et al. [31] and Rodrigues et al. [29] studied the influence of the final carbonization temperature (from 400 °C to 600 °C) on the performance of CMSMs produced from a commercial cellophane precursor. Increasing the CMSMs carbonization temperature (from 550 °C to 600 °C), the permeability to O_2 decreased from 4.33 to 0.23 barrer and the O_2/N_2 permselectivity increased *ca.* 7 times [31]. Rodrigues et al. [29], reported the highest O_2/N_2 permselectivity (>800) with cellulose-based CMSMs; despite this, the permeability to O_2 was quite low (1.33 barrer). Later, in 2018, Rodrigues et al. [28] reported for the first time a tailor-made precursor from cellulose dissolved in a binary mixture of ionic liquid/dimethyl sulfoxide (DMSO). An optimization of the final carbonization temperature allowed them to produce CMSMs (carbonized at 550 °C) with a permeability to O_2 of 5.16 barrer and a O_2/N_2 permselectivity of 32.3.

Post-treatments applied to the carbon membranes have also been used to optimize the separation performance. The exposure of cellulose-based CMSMs to air for one year was shown to render them more permselective for the O_2/N_2 separation: the ideal selectivity increased from 30 to 52, though the permeability to oxygen decreased from 5.1 to 1.9 barrer [32]. In this work, the authors concluded that storing the CMSMs in a propylene atmosphere for 10 days allow to produce membranes that remained stable to oxygen chemisorption for more than 1 year, while the permeability to O_2 was not impaired [32]. Furthermore, feeding with propylene a membrane module for 24 h allowed to increase the permeability to O_2 from 5.13 to 22.2 barrer and the O_2/N_2 selectivity from 30.2 to 40.7.

In addition to the proper selection of the polymeric precursor, carbonization conditions and post-carbonization treatments, the precursor pre-treatment (pre-carbonization treatments) should be considered. Lei et al. [33,34], fabricated carbon hollow fiber membranes (CHFM) from microcrystalline cellulose dissolved in the same solvent solution as reported by Rodrigues et al. [28]. The preparation conditions of the precursor were optimized and allowed to achieve a permeability to O_2 15 times higher than the obtained by Rodrigues et al., though for the obtained O_2/N_2 permselectivity was half of the one obtained by Rodrigues et al. [33]. Lei et al. [35], also demonstrated a process to increase the selectivity which consists of drying the cellulose precursor, up to 140 °C, to remove the glycerol and water used in the coagulation bath. Replacing water molecules by glycerol prevents pores to collapse during the drying process [35] and glycerol seems to act as a pore forming agent, enabling a carbon membrane with larger micropores [35]. The precursor dried at RT originated, after carbonization, CHFMs with a permeability to O_2 of ca. 300 barrer and with a O_2/N_2 permselectivity of *ca.* 7.5; by comparison, the precursor dried at 140 °C originated CHFMs with a permeability to O_2 of *ca.* 22 barrer and a *ca.* 3-fold higher O_2/N_2 permselectivity [35]. Regarding the CO_2/CH_4 permselectivity, the pre-drying technique allowed to increase *ca.* 10-fold. The same authors reported for the first-time asymmetric cellulose based CMSMs with a thin selective skin [22].

CMSMs produced from cellulose have a relatively high amount of oxygen heteroatoms which are intimately related to the high selectivities that these membranes exhibit, as concluded in our previous work [32]. On the other hand, doping carbon with nitrogen heteroatoms is a strategy that has been used to increase the sorption capacity to O_2 or to CO_2 molecules, increasing the separation performance [36–38]. To et al. [36], reported the development of activated carbons doped with nitrogen groups that allowed to increase not only the CO_2 adsorption capacity, but also the micropore volume and the selectivity for CO_2/N_2 separation. Activated carbon doped with nitrogen functional groups can be produced by the thermal decomposition of materials such as urea, melamine, cyanamide and pyridine among others [39,40]. These materials have been widely studied for the oxygen reduction reaction, for replacing the platinum-based catalysts, due to their higher concentration of active sites with high affinity for oxygen [41–43]. Therefore, this work aims at to increase the separation performance of cellulose-based CMSMs to CO_2 and O_2 by doping the precursor with urea, a low-cost source of nitrogen. Urea has an excellent affinity for cellulose and it is widely used to form precursor solutions to regenerate cellulose for film production [44–46] and produce nitrogen-doped porous carbon for supercapacitors [47,48]. Urea was also added to a chitosan precursor (an amine-containing cellulose analogue) to produce carbon adsorbents with an increased volume of ultra-micropores (pore size < 1 nm) and an increased CO_2 adsorption capacity [38].

This work demonstrates, for the first time, the addition of urea to the cellulose precursor solution to produce N-doped CMSMs with a higher micropore volume and with improved permeability to O_2 without compromising the O_2/N_2 selectivity. The addition of nitrogen was confirmed by elemental analysis and the C–N bonds were observed by XPS. The ability of urea to act as a pore forming agent, and the tuning of pore size by changing the urea concentration in the precursor solution, was demonstrated by SAXS and CO_2 adsorption isotherms. This combination of N-doping and tuning of pore size allowed to increase the sorption capacity of O_2 and CO_2 species in membranes without compromising the N_2 sorption, and so preserve the high selectivity of these membranes, as illustrated by the adsorption isotherms of these species. The membranes reported here showed excellent separation performance for producing oxygen enriched air streams, for CO_2 separation from natural gas/biogas and for the recovery of H_2 from hydrocarbon streams.

2. Experimental

2.1. Materials

Wood pulp, with a degree of polymerization of 450, was provided by Innovia Films Ltd. Dimethyl sulfoxide (DMSO) (99.9%) was purchased from Fisher Scientific. The ionic liquid, 1-ethyl-3-methylimidazolium acetate (Emimac) (≥95%) and urea were purchased from Sigma-Aldrich. Hydrogen (99.999%), carbon dioxide (99.998%), oxygen (99.995%), nitrogen (99.999%) and methane (99.995%) were supplied by Air Liquide.

2.2. Fabrication of urea doped cellulose based precursor

Wood pulp (9.2 wt%) and urea (0–2.8 wt%) were dissolved in Emimac:DMSO (30:70 wt%) by magnetic stirring for *ca.* 2 h at 90 °C. Three different urea concentrations (0, 1.4 and 2.8 wt%) were used to prepare the urea doped CMSMs. The Emimac:DMSO ratio of 30:70 wt% was reported to be ideal for solubilizing cellulose and producing high performance CMSMs [28,35]. The resulting cellulose homogeneous mixture was degassed in a vacuum oven for 2 h at 40 °C. Before casting the

polymeric precursor film, the mixture was heated to 60 °C to reduce the viscosity. The polymeric precursor films were coated on square glass plates (10 × 10 cm^2) with a spin coater (POLOS™, SPIN150i). The spin rate used for preparing the cellulose/urea films was 1200 rpm with an acceleration of 1000 rpm s^{-1} for 10 s. The coated cellulose films were coagulated in distilled water at room temperature. The water was replaced at least 6 times for excess of solvent removal, during 1 h. The films were left to dry overnight (*ca.* 18 h), coated in the glass plate, at room conditions. Detailed description of this procedure can be found elsewhere [28].

2.3. Carbon membrane preparation

The dried cellulose-urea doped precursor films were cut in disks with a diameter of 53 mm and placed in a horizontal stainless-steel grid. The precursor films were then carbonized at 550 °C in a horizontal furnace (Termolab TH) equipped with a quartz tube, following the temperature history used in our previous work [32]. Nitrogen or carbon dioxide were used as purge gases with a continuous flow rate of 170 mL min^{-1}. Carbon dioxide was used preferentially to nitrogen because, as reported in Ref. [35] and confirmed in this work, produces CMSMs with a higher micropore volume. Before removing the CMSMs, the furnace was left to cool down naturally to the room temperature. Immediately after the carbonization, the prepared CMSMs were glued to a circular stainless-steel foil support with an inner concentric circular aperture, with an epoxy glue (Araldite® rapid). After 2 h, required for the glue cure completely, the supported CMSMs were placed inside the permeation cell. The prepared CMSMs are named by their concentration of urea in the precursor solution – carbon membrane urea (CMU); CMU-0 was prepared with 0 wt% of urea, CMU-1.4 with 1.4 wt% and the CMU-2.8 with 2.8 wt% of urea.

2.4. Gas permeation measurements

The single gas permeation experiments were performed at 25 °C and *ca.* 1 bar of feeding pressure using the traditional time-lag method. The permeation cell was placed inside a thermostatic cabinet. The entire system was evacuated using a rotary vacuum pump (Edwards, RV5) until a pressure of *ca.* 30 mbar. The permeate gas tank has a volume of 69.2 cm^3.The permeability to H_2, N_2, CO_2, CH_4 and O_2 was obtained by this order, to prevent early chemisorption by oxygen. Each permeation experiment took *ca.* 24 h. At least 3 different CMSMs were tested to evaluate the average gas permeability. The permeability of the CMSMs was computed from the time derivative of the permeating pressure assuming ideal gas behavior. The permeability of a membrane, L_i, was calculated from equation (1):

$$L_i = \frac{2.69 \times 10^{-3}\,\delta\,V}{T\,A_M\,(p_f - p_p)} \bullet \left(\frac{dp}{dt}\right) \quad (1)$$

where δ is the membrane thickness, V is the volume of the permeate tank, T is the absolute temperature, p_f and p_p are the feed and the permeate pressure, respectively and t is the time. The permselectivity, $\alpha_{i,j}$, of the CMSMs was calculated from the permeability ratio of gas species i and j. Detailed information about gas permeability and the respective Robeson Index calculation can be found elsewhere [32]. The gas permeability was expressed in barrer (1 barrer = 3.39 x 10^{-16} mol m m^{-2}•s^{-1} Pa^{-1}).

2.5. Characterization

Scanning electron microscopy (SEM) images were obtained from the cellulose-urea precursor films and respective CMSMs using a Phenom XL SEM. The samples were coated with Au/Pd using a Leica EM ACE2000 Sputter Coater equipment, before being analyzed. The thickness of the CMSMs were obtained with high accuracy using a digital micrometer, Mitutoyo MDH-25 M, and confirmed by SEM. The CMSM shrinkage ratio was determined by the difference in the CMSMs outer diameter before and after the carbonization procedure, as described elsewhere [28].

Atomic Force Microscopy (AFM) was used to study the CMSM surface, using an atomic force microscope from Agilent Technologies (molecular imaging) with a close-loop 5500 (Pico+) system & Large Samples 5500LS (PicoMAPS) system.

Scanning Transmission Electron Microscopy (STEM) was used to obtain micrographs of structure of the prepared CMSM. A Probe-corrected STEM Titan ChemiSTEM was operated at 200 kV and the micrographs were obtained with 80 pm of resolution.

Thermogravimetric analysis was performed in a thermogravimetric balance (NETZSCH STA 449 F3 Jupiter) under 30 mL min^{-1} continuous nitrogen flow from room temperature until 600 °C, with a heating rate of 10 °C•min^{-1}. Samples of *ca.* 8 mg were used. The mass derivative was computed to determine the precursor decomposition temperature.

Fourier Transform Infrared Spectroscopy (FTIR) spectra of the precursor films and respective CMSMs were obtained using a VERTEX 70 FTIR BRUKER spectrometer with a high sensitivity DLaTGS detector. The FTIR spectra of the precursor films were obtained in ATR mode. The FTIR spectra of the CMSMs were obtained in transmittance mode using membrane pellets prepared by diluting 1 wt % of the sample in potassium bromide (KBr). Both spectra were recorded from 4000 to 400 cm^{-1} with a resolution of 4 cm^{-1}.

Elemental analysis was used to determine the bulk chemical composition of the prepared polymeric precursors and respective carbon membranes. Carbon (C), hydrogen (H), nitrogen (N) and sulfur (S) contents were determined using a Vario Micro Cube analyzer (Elementar GmbH) at 1050 °C; and the oxygen (O) content was obtained in a Rapid Oxy Cube analyzer (Elementar GmbH), by pyrolysis at 1450 °C.

Water contact angles were measured using the sessile drop method (DataPhysics OCA Series).

Small-angle X-ray scattering (SAXS) measurements were carried out using a Xeuss 2.0 instrument (Xenocs, Grenoble France) located at University of Sheffield. The X-ray beam (9.24 keV) size was 600 μm vertically and 400 μm horizontally, with a distance of 305 mm between sample position and the detector (Pilatus3R 1 M 2D, Dectris, Switzerland). A Liquid gallium X-ray source (MetalJet Excillum, Sweden) was used. Microporous morphological structure of the produced CMSMs was analyzed at intermediate Q values (1.2–10 nm^{-1}) fitting the Teubner-Strey model to the experimental data using the data experimental tool in Sasview 4.2.

X-ray diffraction (XRD, PANalytical X'Pert Pro) operating in Bragg-Brentano focusing geometry and using Cu Kα radiation at wavelengths Cu Kα1 = 1.5406 Å and Cu Kα2 = 1.54443 Å was used to determine the crystallinity index (I_{Cryst}) and the *d*-spacing. The data was collected at 2θ angles (7–60°), with a step size of 0.017°. The crystallinity index (I_{Cryst}) of the cellulose-urea precursor film were calculated as described by Segal et al. [49] by the following equation:

$$I_{Cryst} = \frac{I_m - I_{am}}{I_m} \quad (2)$$

where I_m is the scattered intensity at the main peak (at $2\theta = 20.1°$) and I_{am} is the scattered intensity related to the amorphous region (located at $2\theta = 14.5°$ [35,50]. The crystallite sizes of the prepared cellulose precursor films were computed using the Scherrer equation [51]. The interlayer distance, also known as *d*-spacing of the CMSMs was calculated using the Bragg equation:

$$d = \frac{n\lambda}{2\sin\theta} \quad (3)$$

where d is the *d*-spacing, n an integer number, λ the X-ray wavelength and θ the diffraction angle [52]:

Micropore characterizations were obtained by fitting the adsorption equilibrium isotherm of CO_2 at 273 K (obtained by the volumetric

method as described elsewhere [29,53]) to the Dubinin-Astakhov (DA) equation [54]:

$$\frac{w}{w_0} = exp\left[-\left(\frac{RTln\, p_0/p}{\beta E_0} \right)^n \right] \quad (4)$$

where w is the micropore volume, w_0 is the total micropore volume, E_0 the characteristic adsorption activation energy, p is the pressure, p_0 is the vapor pressure of the free liquid, β is the affinity constant, R is the gas constant, T is the absolute temperature and n is a fitting parameter (for $n = 2$ the DA equation renders to the Dubinin-Raduschkevisch (DR) equation) [55]; for CMS materials, $n \sim 3$ [56].

The CMSMs true density (ρ_s) was measure by helium pycnometry using the volumetric method and the CMSMs bulk density (ρ_b) was determined using the following equation [35]:

$$\frac{1}{\rho_b} = \frac{1}{\rho_s} + w_0 \quad (5)$$

Micropore size distribution (MSD) of the prepared samples were obtained using the method proposed by Nguyen for the determination of the MSD in carbonaceous materials. Detailed information about this method can be found elsewhere [29,57,58].

X-ray photoelectron spectroscopy (XPS) spectra of the CMSMs were acquired using a ESCALAB 250Xi (Thermo Fisher Scientific) XPS spectrometer with a base pressure below $5x10^{-10}$ mbar. A hemispherical analyzer with energy resolution of 0.1 eV with an analysis area of ~0.65 mm^2, defined by the X-ray spot size on the sample, was used. Monochromated Al Ka (hn = 1486.68 eV) was used as X-ray source, operated at 225 W, 15 kV. The XPS spectra were collected at pass energies of 100 eV for the survey spectra and 40 eV for the individual elements.

The Raman spectra of the CMSMs were obtained using a WITEc alpha300 R Confocal Raman with an excitation wavelength of 532 nm. The XPS spectra and Raman peaks were deconvoluted using CasaXPS software.

The adsorption equilibrium isotherms of CO_2, O_2 and N_2 were determined by the volumetric method at 25 °C and up to 7 bar, as described elsewhere [53]. Langmuir (6) and Dual-Site Langmuir (7) equations were fitted to the experimental adsorption data:

$$q = q_s \frac{bP}{1 + bP} \quad (6)$$

$$q = q_{s,1} \frac{b_1 P}{1 + b_1 P} + q_{s,2} \frac{b_2 P}{1 + b_2 P} \quad (7)$$

where q is the adsorbed solute concentration at pressure P; q_s is the adsorbed saturation concentration; b is the adsorption affinity, related to the adsorption strength [59]. The sorption-diffusion model can be used to determine the permeability of CMSMs [32,59]. The sorption coefficients, S, of the gases were determined dividing the adsorbed solute concentration (q) to the permeation pressure (*ca.* 1 bar). The diffusion coefficients, D, *i.e.* the kinetic terms that measure the mobility of gases across the membrane, were calculated using the following equation [35]:

$$D = \frac{P}{S} \quad (8)$$

3. Results and discussion

3.1. Thermogravimetric and structural properties of CMSM precursor

Solutions of the cellulose precursor, with three different concentrations of urea (0, 1.4 and 2.8 wt%), were prepared to fabricate the corresponding CMSMs. The viscosity of the solutions was found to increase with the urea concentration. The maximum urea concentration was found to be 2.8 wt%, due to the extreme increase of viscosity.

Thermogravimetric analysis (TGA) was performed under an N_2 atmosphere to evaluate the thermal stability and decomposition kinetics of the prepared urea-cellulose precursors. The TGAs curves of the three precursors are plotted in Fig. 1A; it can be seen that all samples have the same four distinct zones of mass loss, as reported by Lei et al. [35]. The first zone, up to *ca.* 120 °C, corresponds to the removal of free water from the precursor; the second zone, between 120 °C and 250 °C, corresponds to the release of urea; between 250 °C and 340 °C the cellulose carbonization on-sets with the formation of the pore network, most of the mass is lost in this temperature range; above 340 °C, further degradation of the cellulose occurs and the pore network begins to organize. The derivative of thermogravimetric analysis of precursor films are plotted in Fig. S1. TGA curves of the pristine wood pulp and urea used in this work are plotted in Fig. S2, for reference. SEM images of the surface of the prepared dried precursor films are presented in Fig. S3. Some fiber-like structures can be seen in the membranes processed with urea, which are a consequence of the greater viscosity and heterogeneity of the corresponding precursor solutions.

Table 1 summarizes the main characteristics of the CMSMs precursors from the cellulose precursors with three different urea contents. It can be observed that the average decomposition temperature slightly decreases from 349 °C to 347 °C as urea concentration increases; additionally, the residual mass at 550 °C also decreases with increasing urea concentration.

The structure of the dried precursor films was analyzed using X-ray diffraction (XRD). Fig. 1B shows the characteristic peaks for the cellulose precursor samples. The peaks are located at 2θ *ca.* 12°, 20° and 21°, which correspond to planes (1 $\bar{1}$ 0), (110) and (020), respectively [60,61]; these planes are characteristic of cellulose II [60]; The crystallinity index of the precursors can be calculated using equation (2). This figure also shows that increasing the urea concentration, the intensity of the peaks corresponding to planes (110) and (020) decrease and the intensity of the peak corresponding to the plane (1 $\bar{1}$ 0) increases and the crystallinity index (I_{Cryst}) of the precursors decreases from 54.1% to 47.3%. Urea has the ability to reduce the crystallinity of cellulose through Van der Waals forces, as reported by Fauziyah et al. [62]. The surface scanning electron microscopy (SEM) images of the prepared urea doped CMSMs precursors are presented in Fig. S2. The average size of the cellulose crystallites was calculated from the full width at half maximum (FWHM) of the various diffraction peaks and by the Scherrer equation and the results are presented in Table 1. The addition of urea increased the average size of the cellulose crystallites from 2.86 nm, in the precursor prepared without urea, to 4.07 nm, in the precursor prepared with 2.8 wt% urea.

The bulk chemical composition of the final polymeric precursor films, as determined by elemental analysis, is indicated in Table 1. The elemental analysis shows that although the nitrogen concentration in the films increases with the added amounts of urea, the nitrogen concentration values are quite low. This suggests that most of the urea molecules are removed during coagulation and washing in water. Li et al. [63] found that, in cellulose/urea/NaOH films regenerated in water, the hydrogen bonds linking urea molecules to the –OH groups of cellulose were broken when in contact with water. Then, the urea molecules form clusters in the regenerated film that were later replaced by clusters of water molecules filling the pore and thus creating a more porous regenerated cellulose matrix. The 0.03 wt% of nitrogen found in the precursor film without urea can be attributed to the ionic liquid that was not completely washed away from the film [22]. The higher amount of nitrogen present in the precursor films with 1.4 and 2.8 wt% urea was attributed to urea that remained inside the film, either physically trapped inside some pores or covalently bonded to cellulose, assuming that some reaction may occur during precursor solution preparation.

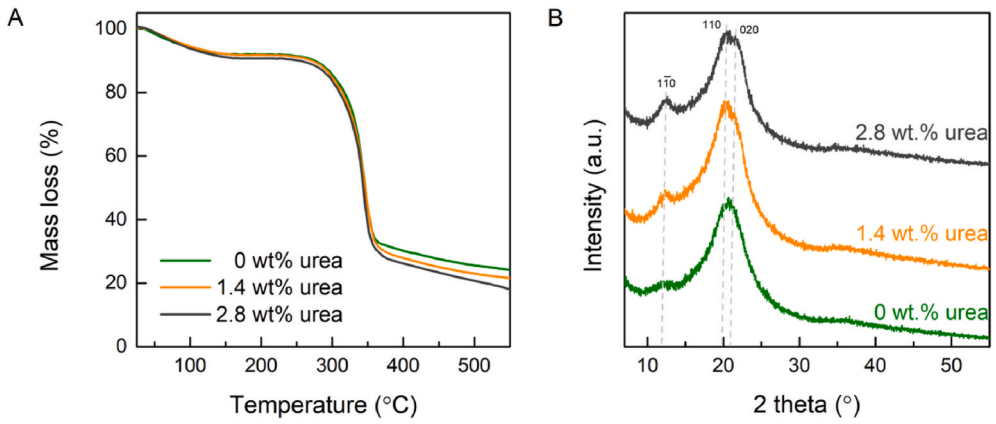

Fig. 1. A) TGA and B) XRD of the cellulose-urea precursor films. (A colour version of this figure can be viewed online.)

Table 1
Main characteristics of the CMSMs precursors for the three urea contents.

		0 wt% urea	1.4 wt% urea	2.8 wt% urea
Decomposition temperature (°C)		349	348	347
Residual mass at 550 °C (%)		24.1	21.4	18.0
Crystallinity index (I_{Cryst}) (%)		54.1	50.4	47.3
Crystallite size (nm)		2.86	3.20	4.07
Bulk composition	**C (%)**	41.5	41.0	40.8
	N (%)	0.03	0.06	0.07
	O (%)	51.8	52.2	52.4
	H (%)	6.76	6.74	6.64

3.2. CMSMs morphology, microstructure and surface chemistry

The precursors analyzed in section 2.1 were carbonized at 550 °C in a carbon dioxide atmosphere. The cellulosic precursors shrank during the carbonization process [28]. Table 2 shows that this shrinkage decreases, from 34.6% (CMU-0) to 30.8% (CMU-2.8), as the urea content in the precursor increases; CMSM samples prepared with the highest urea concentration – 2.8 wt% – should display the highest porosity. The smaller shrinkage value in CMU-2.8 indicates that these membranes have a less dense structure [35]. This phenomenon was assigned to the viscosity increase of the precursor which, during the film formation makes the cellulosic chains get more disorganized and, upon the carbonization stage to display more open pores and a lower density. This phenomenon has been previously reported by other authors [64]. From Table 2, it can also be concluded that the thickness of the CMSMs increases as the urea concentration increases, from 18.3 μm to 23.4 μm. This was assigned to the viscosity increase of the precursor solution, which originates thicker deposited films of the cellulose solution.

The cross-section of the prepared CMSMs were analyzed by SEM, *cf.* Fig. 2A-C; The surface of the samples becomes rougher for higher urea concentrations, as shown in Fig. S4A-D. The surface of CMSMs CMU-0 and CMU-2.8 were also analyzed by atomic force microscopy (AFM), *cf.* Fig. 2D-E; CMU-0 has a smooth surface (Fig. 2D) unlike the surface of the CMU-2.8 (Fig. 2E). Both SEM and AFM results strongly suggest that urea increases the structural disorder of the CMSMs. High resolution scanning transmission electron microscopy (STEM) micrographs were taken to the CMU-0 and CMU-2.8 to observe the carbon membranes microstructure. The micrographs are shown in Fig. 2F-G. These figures reveal that the structure of the prepared carbon membranes is turbostratic and no major changes in the microstructure are observed. However, Fig. 2G suggests a slight alignment of the carbon sheets.

Fig. 2H shows the Small-angle X-ray scattering (SAXS) intensity versus scattering vector curve in a log-log scale of the prepared CMSMs. In the zone of lower Q values (*ca.* $< 1.2\ nm^{-1}$), it is possible to assess the morphology of the materials and in the zone of higher Q values it is possible to assess the microstructure characteristics of the carbon material [65]. In the region of smaller angles, *i.e.*, for the lowest Q values, the signal SAXS intensity increases with the urea concentration. In the micropores region, the SAXS data can be fitted with a Teubner-Strey model, originally developed for microemulsions [65,66], so that this model has been used to assess the microporosity of the different CMSMs; we note that this model has been previously used to model the SAXS data of other disordered carbonaceous materials [53]; the model was run using software SasView5.

The interlayer distance (d-spacing) of the CMSMs were also assessed by XRD and the results are shown in Fig. 2I. Although the d-spacing presented in Fig. 2I is not an effective measure of the pore size of the CMSMs, it indicates the distance between neighboring carbon layers [52]. Fig. 2I shows the plane (002), characteristic of the graphitic domains (sp^2 carbon), at $2\theta \approx 24°$ [22,52]. This figure shows that the d-spacing remains approximately constant and insensitive to the urea content of the CMSMs precursors.

Fitting the Teubner-Strey model to the SAXS results in the micropore region (*i.e.* $1.2 < Q < 10\ nm^{-1}$) it was possible to determine several structural parameters of the prepared CMSMs. According to the best knowledge of the authors, although SAXS has been previously used to study other carbon-based materials this is the first report on the use of SAXS to study the bulk microporous morphology of CMSMs thus opening the door to the use of this powerful characterization technique, in this research field [65]. Using the Teubner-Strey model it is possible to determine the volume fraction occupied by the micropores, φ, the domain size, dz, (*i.e.* the average pore-pore distance) and the correlation length, ξ. From these parameters it is possible to calculate the average radius of the micropores, r, and the internal surface area of the micropores, S_{mp}. Δ SLD is the scattering length density (SLD) difference between the carbon matrix and the pores (the pores have SLD = 0). The SLD of the carbon matrix is calculated from the structural density of the sample using software SasView5. The model equations used in the SasView5 software are indicated in Supplementary Note 1. The characterization parameters obtained applying this model to the SAXS results, for the 3 samples, are indicated in Table 3.

As it can be seen from Table 3, the volume fraction of micropores in the carbonized membranes increases with the urea concentration. The internal surface area of the micropores also increases with the addition of urea, from 946 $m^2\ g^{-1}$ (CMU-0) to 1349 $m^2\ g^{-1}$ (CMU-2.8). Regarding the pore-pore distance and average pore radius, these parameters also

Table 2
Main characteristics of the carbonized CMSMs for the three urea contents.

	CMU-0	CMU-1.4	CMU-2.8
CMSM thickness (μm)	18.3	21.5	23.4
Shrinkage ratio (%)	34.6	32.7	30.8

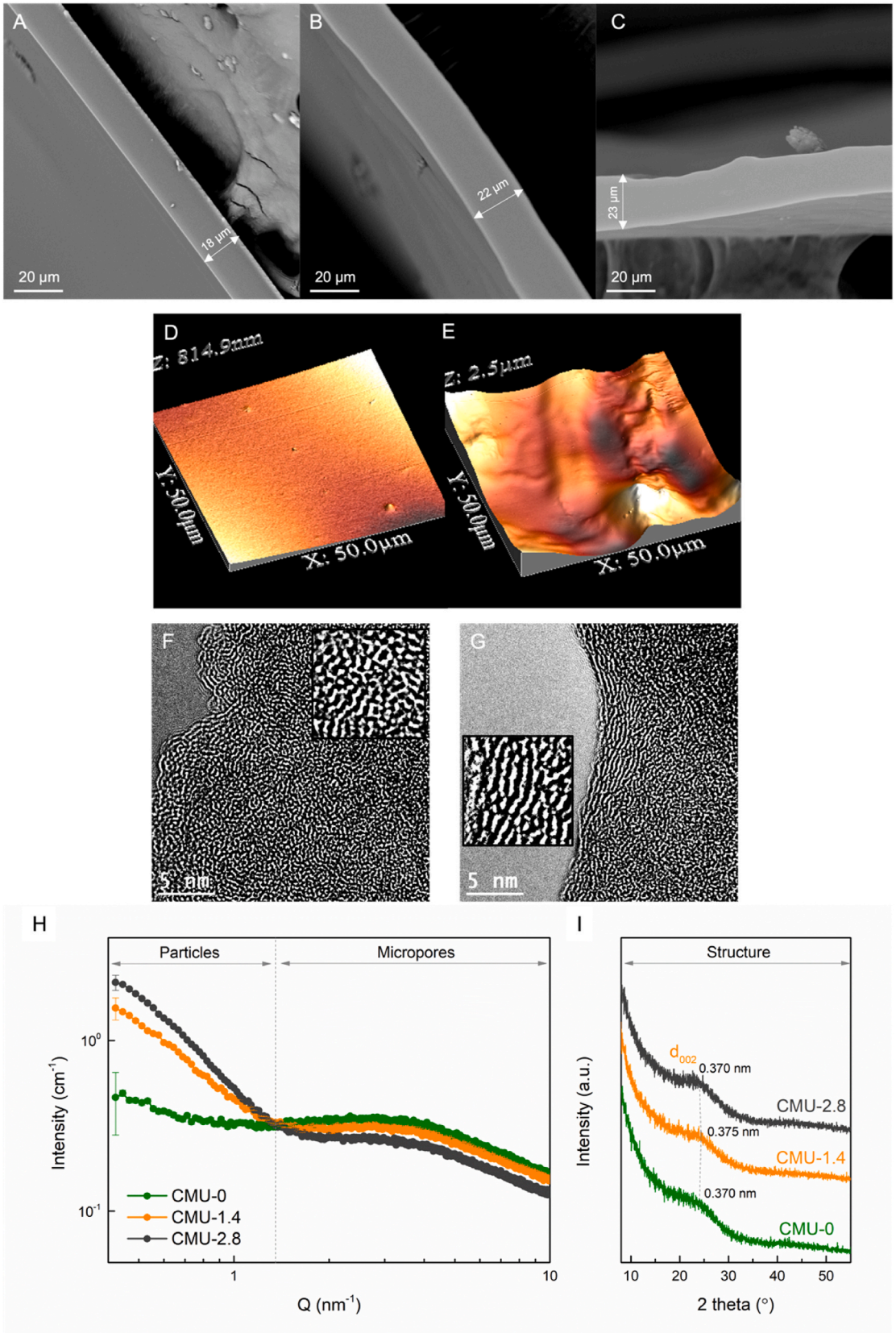

Fig. 2. A-C) Cross-sectional SEM images of CMSMs CMU-0, CMU-1.4 and CMU-2.8; AFM images of the CMU-0 (D) and CMU-2.8 surface (E); F-G) STEM micrographs of CMU-0 and CMU-2.8, respectively; H) SAXS spectra and I) XRD spectra of the produced CMSMs and respective *d*-spacing. (A colour version of this figure can be viewed online.)

Table 3
Morphological parameters of the prepared CMSMs obtained from the SAXS analysis.

	Δ SLD (x10^{-4} nm^{-2})	φ (%)	dz (nm)	ξ (nm)	r (nm)	S_{mp} ($m^2 \cdot g^{-1}$)
CMU-0	18.5	11.3	1.53	0.195	0.225	946
CMU-1.4	16.0	13.4	1.55	0.193	0.236	1275
CMU-2.8	15.6	13.2	1.65	0.180	0.282	1349

Table 4
Micropore structural characterization based on the parameters from DA equation fitted to CO_2 adsorption isotherms at 0 °C.

	ρ_s ($g \bullet cm^{-3}$)	ρ_b ($g \bullet cm^{-3}$)	w_0 ($cm^3 \bullet g^{-1}$)	E_0 ($kJ \bullet mol^{-1}$)	↕$_0$ (nm)
CMU-0	2.173	1.542	0.188	33.14	0.742
CMU-1.4	1.887	1.340	0.214	32.16	0.766
CMU-2.8	1.839	1.285	0.234	32.54	0.746

increase with the addition of urea. Regarding the pore radius, the carbonized CMSM prepared with 2.8 wt% of urea displays an increase of 25% in the pore radius when compared with the sample without urea. These conclusions should, however, be taken with precaution since the SAXS analysis averages crossing as well as dead-end pores, where these latter do not contribute for the membrane permeability.

The pore size distribution and the micropore volume were also obtained from CO_2 adsorption equilibrium isotherm at 0 °C [28]. Fig. 3A shows the CO_2 adsorption isotherm for the prepared CMSMs. The CO_2 adsorption saturation capacity of the CMSMs increases with the urea content. The Dubinin-Astakhov's equation (DA equation) was fitted to the experimental data and the micropore volume (w_0) and the characteristic energy of adsorption (E_0) were obtained and are given in Table 4. The mean pore size (↙$_0$) of the prepared carbon membranes was obtained from the average of the micropore size distribution.

The structural density (ρ_s) and the bulk density (ρ_b) of the prepared CMSMs decrease when the urea concentration in the precursor increases from 0 to 2.8 wt%. This suggests that urea acts as a pore-forming agent, increasing the free volume fraction; actually, it was observed that the micropore volume, w_0, increases from 0.188 to 0.234 $cm^3\ g^{-1}$, as the urea concentration increases. The characteristic adsorption energy is lower for CMSMs prepared using urea. This indicates that the potential for interaction between CO_2 and the CMSM walls became stronger with the increase in the volume of micropores and increase in their average pore width which is attributed to the multilayer adsorption [35].

The micropore size distribution was obtained using the method proposed by Nguyen et al. [57,58] for microporous carbon-based materials. Fig. 3B shows the obtained micropore size distribution for the prepared CMSMs. The membranes prepared present a typical bimodal pore size distribution, micropores in a range of 0.7–1 nm and ultramicropores from 0.35-0.70 nm, a distinct characteristic of the CMSMs [67–69]. The obtained micropore size distribution is shifted to the right, towards larger pores, when compared with other cellulose-based CMSMs [22,28,29,31], presenting a smaller volume of ultramicropores [22].

Sample CMU-2.8 presents the highest micropore volume when compared to the other samples; the urea makes the average pore size to increase. The substantial increase in pore volume fraction between 0.7 nm and 0.9 nm indicates that urea acts as an enlarging pore agent; it is then expected that this CMSM shows higher permeabilities. CMU-1.4 shows an average pore size of 0.766 nm higher than that of the CMU-2.8 – 0.746 nm, which could indicate that the selectivities of the CMU-1.4 is lower. It can be concluded that the addition of urea alters not only the chemical structure of the membranes but also their microporous structure. Therefore, pore tuning can be done by adding urea to the polymeric precursor of CMSMs.

Elemental analysis was used to determine the bulk composition of the prepared CMSMs to confirm the presence of nitrogen in their composition. The results of the elemental analysis are shown in Table 5. In the bulk composition of the carbon membranes, they are mostly composed of carbon and oxygen. The amount of nitrogen increases with the concentration of urea that was added to the polymeric precursor solution. An increase in nitrogen of more than 11% was observed in the carbon membrane prepared with 2.8 wt% of urea.

X-ray photoelectron spectroscopy (XPS) was used to analyze the relative atomic element concentration on the surface of the prepared CMSMs samples. The results are presented in Table 5 and the XPS patterns are plotted in Fig. 4. As shown in Table 5, while the CMSM sample prepared without urea (CMU-0) does not contain any detectable amount of nitrogen, the CMSMs samples CMU-1.4 and CMU-2.8 contain atomic concentrations of nitrogen of respectively ca. 0.38 at.% and 0.52 at.%. The increase in urea concentration in the precursor solution originates CMSMs with a higher atomic concentration of carbon and a lower

Table 5
Atomic concentration on the bulk and at the surface of the produced CMSM.

	Bulk composition				Surface composition		
	%C	%N	%O	%H	%C	%N	%O
CMU-0	88.0	0.05	8.83	3.12	90.4	–	9.60
CMU-1.4	87.7	0.38	8.71	3.21	91.2	0.38	8.46
CMU-2.8	86.8	0.56	9.35	3.29	91.6	0.52	7.84

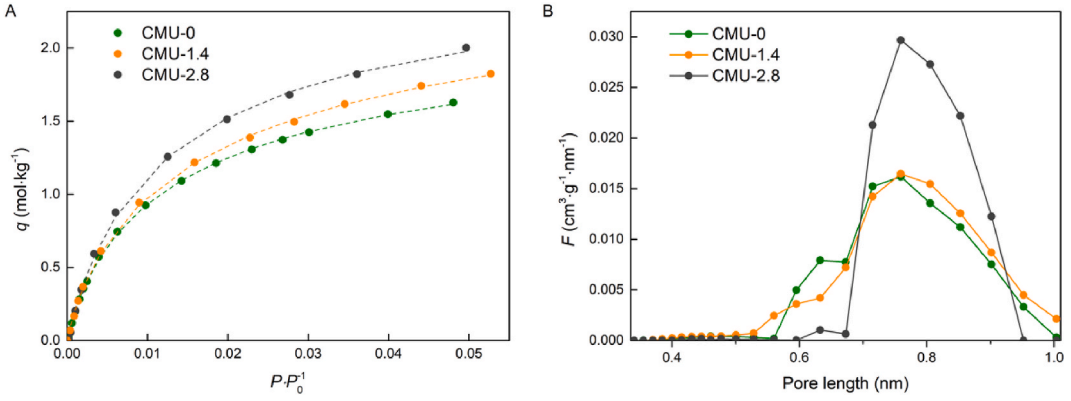

Fig. 3. A. CO_2 adsorption equilibrium isotherms obtained at 0 °C and B. micropore size distribution of the prepared CMSMs obtained from the DA equation. The respective characteristic curves can be found in Fig. S5. (A colour version of this figure can be viewed online.)

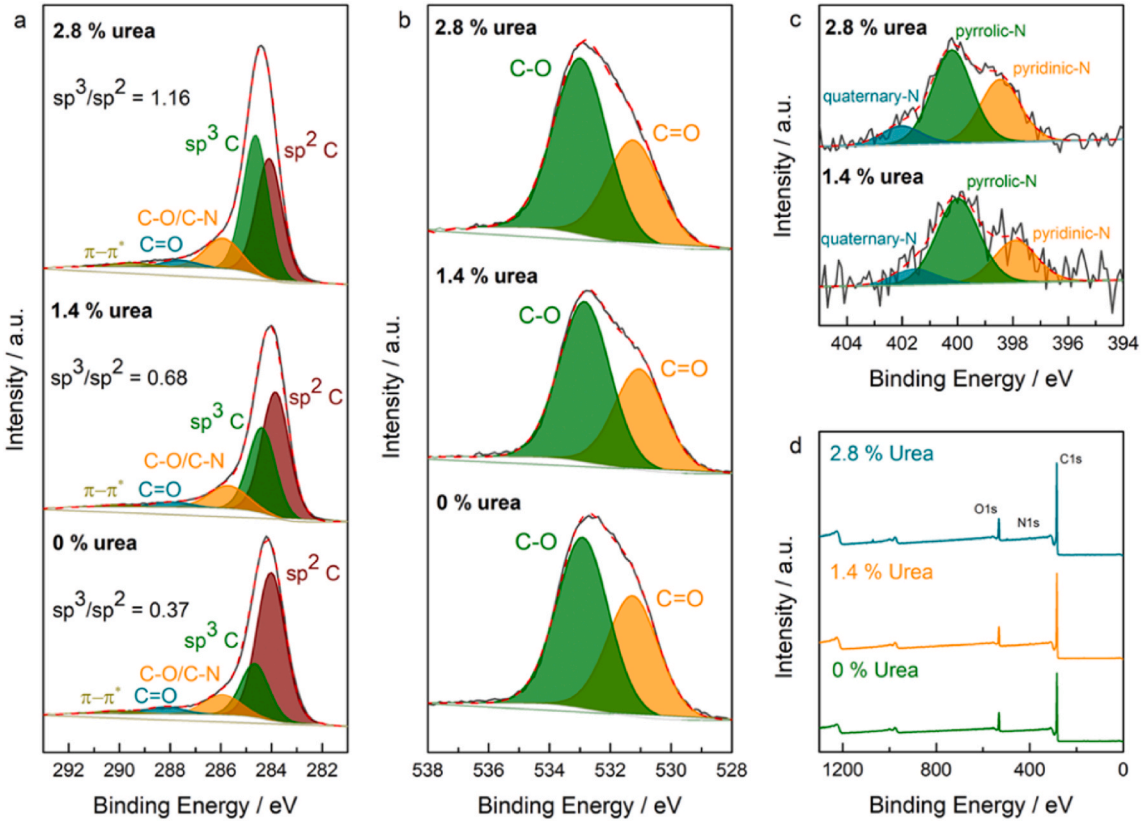

Fig. 4. XPS spectra of a) C1s, b) O1s, c) N1s with the respective deconvoluted peaks and d) the XPS survey of the CMSMs prepared in this work (XPS peak deconvolution results are found in Tables S1–S3.). (A colour version of this figure can be viewed online.)

atomic concentration of oxygen; the C/O ratio increases from 9.42 for CMU-0 to 11.7 for CMU-2.8, cf. Fig. 4d. In our previous work [32] it was concluded that CMSM with a higher C/O ratio display more amorphous carbon and display larger micropores, hence higher permeabilities. Therefore, carbon membrane CMU-2.8 is expected to have higher gas permeabilities. XPS confirms also that covalent C–N bonds are formed due to urea that remained inside the precursor films originating after carbonization, N-doped carbon membranes.

The XPS spectra of C1s region of CMU-0, CMU-1.4 and CMU-2.8 are shown in Fig. 4a. Five peaks per sample were fitted with a consistent protocol as described elsewhere [32]. The prepared CMSMs present a hybrid structure comprising sp^2 and sp^3-hybridized carbon, as reported elsewhere [22,32,70]. Both samples show a peak located around 284 eV binding energy (BE) that is attributed to the sp^2-hybridized carbon, and another peak located at *ca.* 285 eV BE that can be attributed to the sp^3-hybridized carbon. Analyzing the XPS C1s spectra of the prepared CMSMs, the addition of urea promotes an increase in the atomic concentration of sp^3 carbon bonds (C–C). This bond, according to Ma et al. [70], is responsible for forming micropores, *i.e.*, for the imperfect packing of the graphite plates. As observed by the SAXS, the increased concentration of urea in the membranes causes a greater disorder in the carbon structure, hence the presence of larger micropores. The ratio sp^3/sp^2 increases from 0.37 to 1.16 for samples CMU-0 and CMU-2.8, respectively. This indicates that adding urea to the precursor originates membranes where sp^2 carbon domains are partially replaced by sp^3-hybridized carbon, rending the carbon membrane more amorphous [22]. In C1s XPS spectra displays a peak at *ca.* 286 eV BE, which was assigned, in the case of CMU-0, to C–O bonds and the area of this band increases with the addition of urea, indicating that in CMU-1.4 and CMU-2.8 it can be attributed to C–N bonds. Additionally, bands at ~289 eV and ~290 eV were assigned to the C═O bonds and $\pi-\pi^*$ satellite [71].

Regarding the XPS O1s spectra - Fig. 4 b - two characteristic peaks appear with displaying approximately the same areas for the three CMSMs samples. The first, at *ca.* 531 eV, corresponds to C═O binding, while the second peak, at *ca.* 533 eV, corresponds to C–O binding [72]. Fig. 4 c shows the XPS N1s spectra for the samples containing urea, CMU-1.4 and CMU-2.8, respectively. Deconvoluting the spectra, three characteristic peaks were identified: one at *ca.* 398 eV, corresponding to pyridinic-N, one at *ca.* 400 eV, related to pyrrolic-N, and one at *ca.* 402 eV, assigned to graphitic-N [73,74]. As the urea concentration increases, from 1.4 to 2.8 wt %, the relative area of the band corresponding to pyridinic-N also increases, from 29.5 at.% to 36.0 at.%. This increase agrees with previous reports on carbon materials prepared with urea, where it was observed that an increase in urea concentration causes the transformation of pyrrolic-N into pyridinic-N functional groups [75,76]. Pyridinic-N is related to increased sorption of O_2 and CO_2 in N-doped carbon materials [77], so it can be expected that the CMU-2.8 sample has higher gas permeability to O_2 and CO_2 than CMU-0 or CMU-1.4 samples.

The Raman spectra plotted in Fig. 5 shows 5 peaks (G, D1, D2, D3 and D4) were deconvoluted using a protocol described in our previous work [32]. The largest peaks, around *ca.* 1600 cm^{-1}, is known as the G peak and occurs in the graphite band corresponding to the vibration mode of the sp^2-hybridized carbon bonds (E_{2g}-simmetric). Peak D1, at *ca.* 1350 cm^{-1}, corresponds to the vibration mode of disordered graphite (A_{1g}-symmetry) [78,79]. The intensity (area) of the D1 increases with urea content and is indicative of the presence of more defects in the carbon matrix [22,80], in agreement with the SAXS, XRD and XPS results. Furthermore, the increase in intensity (area) of the D2 peak, corresponding to the disordered graphitic lattice vibrations mode, indicates the formation of a more disordered carbon [78,79]. The I_{D1}/I_G ratio increases, from 3.53 to 4.11 – corresponding respectively to CMU-1.4 to CMU 2.8, indicates that the incorporation of urea induces the formation

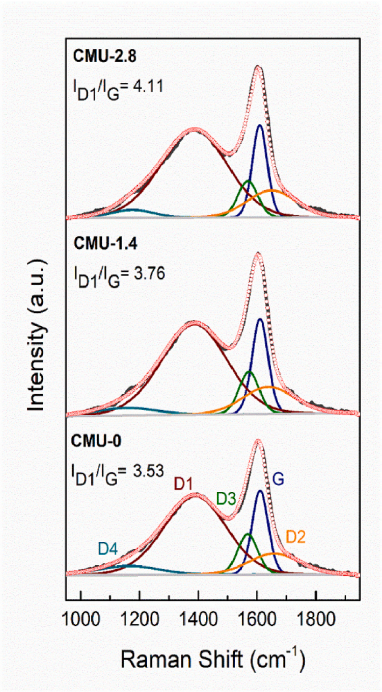

Fig. 5. Raman spectra of the prepared CMSMs with the respective deconvoluted peaks. (Raman peak positions and respective area are presented in Table S4). (A colour version of this figure can be viewed online.)

of a more disordered carbon matrix.

Although XPS confirmed the presence of covalent C–N bonds on the surface of the CMSMs and elemental analysis the presence of nitrogen in the bulk of the CMUs prepared with urea, the formation of graphitic carbon nitride (g-C_3N_4), from the decomposition of urea was not observed. In fact, the XRD of the CMUs (Fig. 2G) indicates that the produced carbon material is amorphous when compared to the spectra of g-C_3N_4 [81].

FTIR analyses and water contact angle measurements of the prepared CMSM are presented in Figs. S6 and S7. From the FTIR analysis of the precursor films (Fig. S6A), no significant band changes were observed with the addition of urea. The FTIR spectra of the CMSMs (Fig. S6B), also do not show relevant differences in the bands, which indicates that the changes induced by urea should be mostly structural. Regarding the water contact angles of the prepared CMSMs (Fig. S7), adding urea increases the water contact angle, from 65° in CMU-0 to 79° in CMU-2.8. Therefore, it can be concluded that urea increases the surface hydrophobicity of the CMSMs.

3.3. Gas permeation results

The prepared CMSMs were synthesized carbonizing precursor films in a carbon dioxide atmosphere at 550 °C. Additionally, some CMSMs were carbonized under a nitrogen atmosphere but these exhibited lower separation performances, as indicated in Table S5. The prepared CMSMs were characterized using single gas permeation experiments at 25 °C and 1 bar of feed pressure and vacuum (30 mbar) in the permeate side. The following gas probes were used: H_2 (kinetic diameter = 0.290 nm), CO_2 (0.335), O_2 (0.346), N_2 (0.378) and CH_4 (0.380 nm). Fig. 6 shows the permeability as a function of the kinetic diameter of the tested gases for the prepared CMSMs; the corresponding permeability values are shown in Table S5.

According to Fig. 6, the permeability of the prepared CMSM depends on the kinetic diameter of the probing gases. The smaller the kinetic diameter of a gas, the greater is the permeability to that gas, which indicates that the transport mechanism is mostly molecular sieve

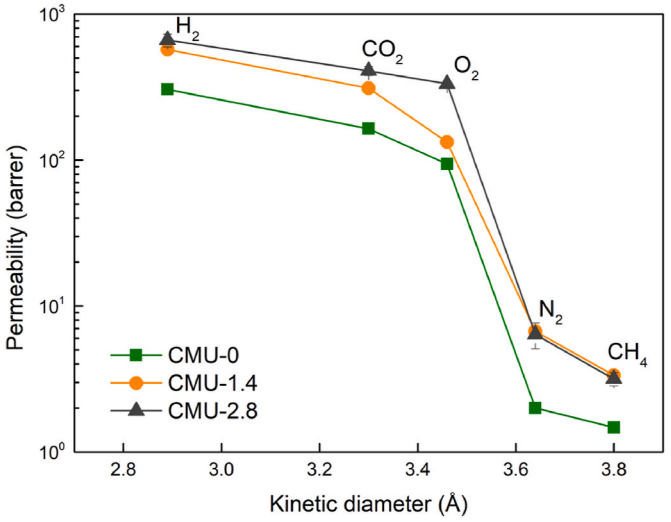

Fig. 6. Single gas permeation of the prepared CMSMs as a function of gas kinetic diameter at 25 °C. The error bars present the gas permeability variance of 3 different CMSMs. (A colour version of this figure can be viewed online.)

mechanism [68]. It can also be concluded that the addition of urea makes the permeability of the prepared carbon membranes to increase: CMU-0 < CMU-1.4 < CMU-2.8. The permeability to H_2 more than doubles from CMU-0 (305 barrer) to CMU-2.8 (664 barrer). A similar behavior is observed for the permeability to the other gas species. However, the largest increase was observed for oxygen, which permeability increased from 94 barrer to 333 barrer for CMU-0 and CMU-2.8 membranes, respectively. These results support the previous observations that adding urea to the precursor changes the micropore volume and increases the average micropore size of the CMSMs.

The permselectivity and respective Robeson Index for the O_2/N_2, CO_2/CH_4 and H_2/CH_4 separations are shown in Table 6. Normally, the increase in the micropore volume and the sp^3/sp^2 ratio would promote a decrease in the permselectivity of the CMSMs [22,70]. But, in this case it was observed that adding 2.8 wt% of urea slightly increased the permselectivity of CMU-2.8 carbon membrane for all tested gas pairs. This effect should be assigned to the presence of nitrogenous functional groups, which increase the adsorption of CO_2 and O_2, thus making the CMSMs more permeable to these gases and more selective; for example, the Robeson Index for the O_2/N_2 separation increased from 8.6 to 12.3, for membranes CMU-0 and CMU-2.8, respectively. The permselectivities of CMU-1.4 are lower than for the other carbon membranes, most likely due to the lower ℓ_0 that these membranes presented. As the Robeson Index values reported in Table 6 are greater than 1, the CMSMs produced in this work are positioned well above the 2008 Robeson Upper Bound limit.

After single-component gas permeation tests, membranes CMU-0 and CMU-2.8 were stored in a laboratory environment for 60 days and for 120 days to assess the impact of aging on their O_2/N_2 separation performance. After 60 days of contact with ambient air, CMU-0 membrane decreased its permeability to oxygen from 94 barrer to 85 barrer, a reduction of *ca.* 9%; and after 120 days its permeability to oxygen

Table 6
CMSMs permselectivity (α) and respective Robeson Index (θ) for O_2/N_2, CO_2/CH_4 and H_2/CH_4.

	O_2/N_2		CO_2/CH_4		H_2/CH_4	
	α	θ	α	θ	α	θ
CMU-0	47.0	8.60	112	2.20	208	3.60
CMU-1.4	19.9	3.90	92.8	2.30	170	5.20
CMU-2.8	53.8	12.3	132	3.60	214	7.60

reduced by *ca.* 13% while the permselectivity increased from 47 to 60. This reduction in permeability to O_2 caused by aging is rather small if compared with the literature values for cellulose-based carbon membranes [22,29,35,82]. In the case of CMU-2.8, the permeability reduction to oxygen was more accentuated, due to the higher chemisorption of oxygen by a nitrogen doped membrane. The permeability to oxygen decreased *ca.* 36% after 60 days and *ca.* 43% after 120 days of contact with air. In this case, the O_2/N_2 permselectivity increased from 42.8 to 130 after 120 days of aging. This increase of approximately 3 times was caused by the decrease of permeability to nitrogen, due to shrinkage of the pores and reduction of active adsorption sites for the molecules to adsorb caused by the irreversible chemisorption of oxygen. Despite this aging, CMU-2.8 membrane continues to be quite competitive when compared to others produced from the carbonization of a cellulose precursor [4,83,84].

Fig. 7 shows the Robeson plot for the O_2/N_2 separation of the CMSMs prepared in this work, compared with the best performing cellulose-based CMSMs, reported in the last decade. Carbon membranes CMU-0, CMU-1.4 and CMU-2.8 exhibit superior separation performance than the state-of-the-art membranes. Remarkably, to the best of the authors' knowledge, CMU-2.8 carbon membrane has one of the highest O_2/N_2 membrane separation performance reported so far in the literature. This CMSM has a selectivity *ca.* 7 times higher than the CMSM reported by Lei et al. [35] which was to date the cellulose-based CMSM with the highest permeability to O_2 (300 barrer). The separation performance results represented in Fig. 7 are shown in Table S6.

3.4. Transport properties

Adsorption equilibrium isotherms of CO_2, O_2 and N_2 were obtained on CMSMs CMU-0, CMU-1.4 and CMU-2.8 at 25 °C and are plotted in Fig. 8. The dashed lines are the Langmuir and Dual-site Langmuir equations fitting lines; the respective fitting parameters are listed in Table S7. Fig. 8 also plots the diffusion coefficients obtained for the three carbon membranes and for the three gases at 25 °C.

The adsorption equilibrium isotherms show nearly the same behavior for all gases. The adsorption capacity at 7 bar for carbon dioxide and oxygen increases as the urea content increases. As discussed before, this effect is assigned to the increase on the pore size and adsorption surface area of the carbon membranes prepared with an increased concentration of urea but also on the pore surface chemistry, which contains an increasing concentration of nitrogenous functional groups. In the case of the nitrogen, the adsorption concentration either stays constant (CMU-0 and CMU.2.8) or decreases slightly (case of CMU-1.4) which favors O_2/N_2 selectivity for membranes CMU-1.4 and CMU-2.8. The sorption coefficients determined at *ca.* 1 bar are listed in Table S8. The carbon dioxide sorption coefficients remain almost constant with the addition of urea; however, oxygen sorption coefficients increase with the urea concentration; and, as expected, the nitrogen sorption coefficients decrease with the addition of urea.

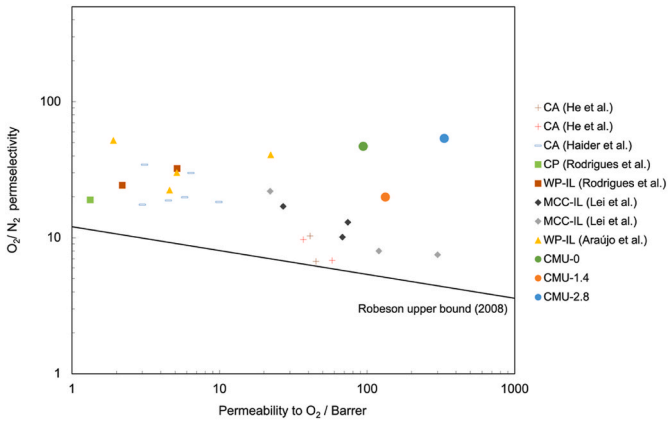

Fig. 7. Comparison of O_2/N_2 separation performance of the produced CMSMs with the state-of-the-art cellulose-based CMSMs. (He et al. [30,85]; Haider et al. [83,86]; Rodrigues et al. [28,29]; Lei et al. [33,35] and Araújo et al. [32]). (A colour version of this figure can be viewed online.)

The transport mechanism in CMSMs can be described by the sorption-diffusion mechanism, where the permeability is given by the product of the sorption coefficient to the diffusion coefficient. Diffusion coefficients were then computed and plotted in Fig. 8D. Carbon membrane CMU-0 has a denser structure; therefore, it has lower diffusivities. The diffusivity of all gases increases from CMU-0 to CMU-2.8. However, the diffusivity of nitrogen slightly decreases from CMU-1.4 to CMU-2.8, from $1.3x10^{-8}$ to $1.2x10^{-8}$ cm^2 s^{-1}.

The separation performance of carbon membrane CMU-2.8 is extremely competitive for producing enriched oxygen air streams useful namely for oxy-combustion processes, medical applications and aquaculture. In addition, these membranes feature interesting results for CO_2/CH_4 separation, such as the biogas upgrading; and for hydrogen recovery from natural gas pipelines (H_2/CH_4) or for hydrogen purification from ammonia processes (H_2/N_2).

4. Conclusions

A simple strategy for pore tuning CMSMs for gas separation is reported. Flat sheet CMSMs were prepared by the controlled carbonization of cellulose precursor doped with 2 different concentrations of urea. Some reference CMSMs were also prepared without urea. The sample with the highest urea concentration, CMU-2.8, displayed the highest permeability to O_2 – 333 barrer– and the highest O_2/N_2 permselectivity – 53.8, Robeson Index of 12.3 – ever reported.

The addition of urea to the cellulose precursor produced polymeric films with a higher structural disorder and with a lower crystallinity. Elemental analysis confirms the presence of nitrogen functional groups on the precursor and respective CMUs. The XPS data shows that C–N covalent bonds were formed. The resultant CMSMs displayed a more disordered carbon structure containing nitrogen functional groups. The increase in the sp^3/sp^2 and I_{D1}/I_G ratio in the CMSMs prepared with urea allowed to increase the micropore volume from 0.188 cm^3 g^{-1} to 0.234 cm^3 g^{-1}, respectively carbon membranes CMU-0 and CMU-2.8. Additionally, there was an increase in the micropore surface area and in the pore radius. Urea changes the morphological structure of polymeric precursors, producing carbon membranes with higher porosity (due to the increase in micropore volume and surface area determined by SAXS and carbon dioxide adsorption isotherm at 0 °C), suggesting that urea acts as a pore-forming agent of CMSMs.

The permeability to O_2 increased from 94 barrer to 333 barrer, respectively for carbon membranes CMU-0 and CMU-2.8, without affecting the O_2/N_2 permselectivity – *ca.* 54. The increase in the permeability without impairing the selectivity was assigned to the nitrification of the micropores inner surface which favors the adsorption of O_2 and CO_2 over N_2. The developed carbon membranes are highly competitive for several applications, namely for producing oxygen enriched air streams for combustion possesses, medical applications and aquaculture – O_2/N_2 ($\theta = 12$); hydrogen recovery from methane – H_2/CH_4 ($\theta = 8$); CO_2 from biogas and natural gas – CO_2/CH_4 ($\theta = 4$); hydrogen recovery from ammonia processes – H_2/N_2 ($\theta = 4$).

CRediT authorship contribution statement

Tiago Araújo: Conceptualization, Methodology, Investigation, Writing – original draft. **Andrew J. Parnell:** Investigation. **Gabriel Bernardo:** Supervision, Writing – review & editing. **Adélio Mendes:** Supervision, Project administration, Writing – review & editing.

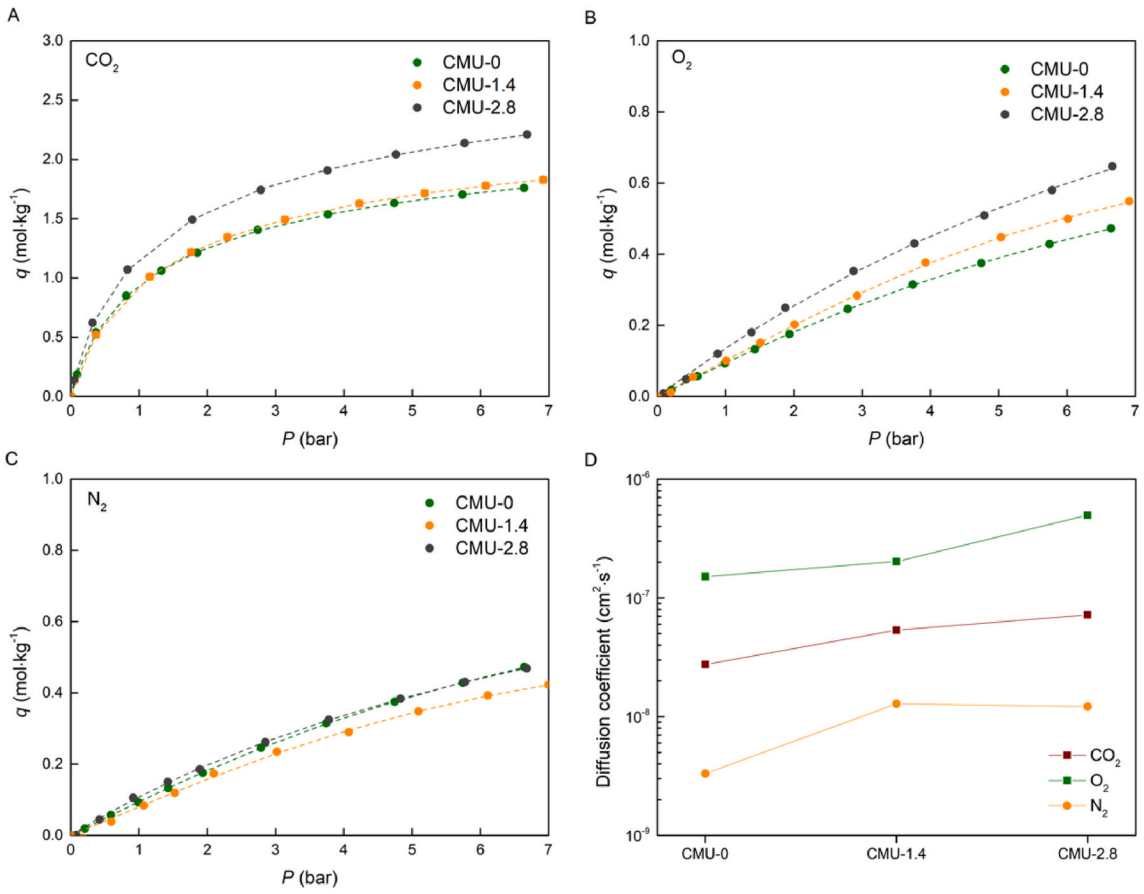

Fig. 8. Adsorption equilibrium isotherms performed at 25 °C until ca. 7 bar of A) CO_2, B) O_2 and C) N_2. D) shows the calculated diffusion coefficients. (A colour version of this figure can be viewed online.)

Declaration of competing interest

The authors declare that they have no known competing financial interests or personal relationships that could have appeared to influence the work reported in this paper.

Acknowledgements

T. Araújo is grateful to the Portuguese Foundation for Science and Technology (FCT) for the doctoral grant (reference SFRH/BD/143598/2019) supported by POPH/FSE. G.Bernardo thanks the Portuguese Foundation for Science and Technology (FCT) for the financial support of his work contract through the Scientific Employment Stimulus Individual Call – (CEEC_IND/02039/2018). This work was financially supported by LA/P/0045/2020 (ALiCE), UIDB/00511/2020 and UIDP/00511/2020 (LEPABE), funded by national funds through FCT/MCTES (PIDDAC). The authors are glad to Innovia Films Ltd. for generously providing the wood pulp.

Appendix A. Supplementary data

Supplementary data to this article can be found online at https://doi.org/10.1016/j.carbon.2022.12.062.

References

[1] A. Sikora, European Green Deal – legal and financial challenges of the climate change, ERA Forum 21 (4) (2020) 681–697.
[2] D.S. Sholl, R.P. Lively, Seven chemical separations to change the world, Nature 532 (2016) 435–437.
[3] H.C. Lau, S. Ramakrishna, K. Zhang, A.V. Radhamani, The role of carbon capture and storage in the energy transition, Energy Fuel. 35 (9) (2021) 7364–7386.
[4] L. Lei, L. Bai, A. Lindbråthen, F. Pan, X. Zhang, X. He, Carbon membranes for CO2 removal: status and perspectives from materials to processes, Chem. Eng. J. 401 (2020), 126084.
[5] K.-K. Wu, Y.-C. Chang, C.-H. Chen, Y.-D. Chen, High-efficiency combustion of natural gas with 21–30% oxygen-enriched air, Fuel 89 (9) (2010) 2455–2462.
[6] U.S.D.o.E.I.H.E. Association, Imporving Process Heating System Performance: A Sourcebook for Industry, Industrial Technologies Program, 2004.
[7] U.S.D.o. Energy, Oxygen-Enriched Combustion, 2005, in: https://www.energy.gov/sites/prod/files/2014/05/f16/oxygen_enriched_combustion_process_htgts3.pdf.
[8] B. Adhikari, C.J. Orme, J.R. Klaehn, F.F. Stewart, Technoeconomic analysis of oxygen-nitrogen separation for oxygen enrichment using membranes, Separ. Purif. Technol. 268 (2021), 118703.
[9] M. Micari, K.V. Agrawal, Oxygen enrichment of air: performance guidelines for membranes based on techno-economic assessment, J. Membr. Sci. 641 (2022), 119883.
[10] R.W. Baker, Future directions of membrane gas separation Technology, Ind. Eng. Chem. Res. 41 (6) (2002) 1393–1411.
[11] G. Bernardo, T. Araújo, T. da Silva Lopes, J. Sousa, A. Mendes, Recent advances in membrane technologies for hydrogen purification, Int. J. Hydrogen Energy 45 (12) (2020) 7313–7338.
[12] X. He, L. Lei, Z. Dai, Green hydrogen enrichment with carbon membrane processes: techno-economic feasibility and sensitivity analysis, Separ. Purif. Technol. 276 (2021), 119346.
[13] L.M. Robeson, Correlation of separation factor versus permeability for polymeric membranes, J. Membr. Sci. 62 (2) (1991) 165–185.
[14] M. Teixeira, M.C. Campo, D.A. Pacheco Tanaka, M.A. Llosa Tanco, C. Magen, A. Mendes, Composite phenolic resin-based carbon molecular sieve membranes for gas separation, Carbon 49 (13) (2011) 4348–4358.
[15] J.S. Adams, A.K. Itta, C. Zhang, G.B. Wenz, O. Sanyal, W.J. Koros, New insights into structural evolution in carbon molecular sieve membranes during pyrolysis, Carbon 141 (2019) 238–246.
[16] P.J. Williams, W.J. Koros, Gas separation by carbon membranes, in: N.N. Li, A.G. Fane, W.S. Ho, T. Matsuura (Eds.), Dvanced Membrane Tecnology and Applications, Wiley-AIChE2008, pp. 599-632.
[17] M.-B. Hägg, X. He, Carbon molecular sieve membranes for gas separation, in: E. Drioli, G. Barbieri (Eds.), Membrane Engineering for the Treatment of Gases:

Gas-separation Problems Combined with Membrane Reactors, The Royal Society of Chemistry, Cambridge, 2011, pp. 162–191.
[18] M. Shah, M.C. McCarthy, S. Sachdeva, A.K. Lee, H.-K. Jeong, Current status of metal–organic framework membranes for gas separations: promises and challenges, Ind. Eng. Chem. Res. 51 (5) (2012) 2179–2199.
[19] Q. Song, S.K. Nataraj, M.V. Roussenova, J.C. Tan, D.J. Hughes, W. Li, P. Bourgoin, M.A. Alam, A.K. Cheetham, S.A. Al-Muhtaseb, E. Sivaniah, Zeolitic imidazolate framework (ZIF-8) based polymer nanocomposite membranes for gas separation, Energy Environ. Sci. 5 (8) (2012) 8359–8369.
[20] S.K. Alen, S. Nam, S.A. Dastgheib, Recent advances in graphene oxide membranes for gas separation applications, Int. J. Mol. Sci. 20 (22) (2019).
[21] T. Araújo, G. Bernardo, A. Mendes, Cellulose-based carbon molecular sieve membranes for gas separation: a review, Molecules 25 (15) (2020).
[22] L. Lei, F. Pan, A. Lindbråthen, X. Zhang, M. Hillestad, Y. Nie, L. Bai, X. He, M. D. Guiver, Carbon hollow fiber membranes for a molecular sieve with precise-cutoff ultramicropores for superior hydrogen separation, Nat. Commun. 12 (1) (2021) 268.
[23] M. Rungta, G.B. Wenz, C. Zhang, L. Xu, W. Qiu, J.S. Adams, W.J. Koros, Carbon molecular sieve structure development and membrane performance relationships, Carbon 115 (2017) 237–248.
[24] J. Koresh, A. Soffer, A molecular sieve carbon membrane for continuous process gas separation, Carbon 22 (2) (1984) 225.
[25] J.E. Koresh, A. Sofer, Molecular sieve carbon permselective membrane. Part I. Presentation of a new device for gas mixture separation, Separ. Sci. Technol. 18 (8) (1983) 723–734.
[26] J.E. Koresh, A. Soffer, The carbon molecular sieve membranes. General properties and the permeability of CH4/H2 mixture, Separ. Sci. Technol. 22 (2–3) (1987) 973–982.
[27] A.F. Ismail, L.I.B. David, A review on the latest development of carbon membranes for gas separation, J. Membr. Sci. 193 (1) (2001) 1–18.
[28] S.C. Rodrigues, M. Andrade, J. Moffat, F.D. Magalhães, A. Mendes, Preparation of carbon molecular sieve membranes from an optimized ionic liquid-regenerated cellulose precursor, J. Membr. Sci. 572 (2019) 390–400.
[29] S.C. Rodrigues, M. Andrade, J. Moffat, F.D. Magalhaes, A. Mendes, Carbon membranes with extremely high separation factors and stability, Energy Technol. 7 (4) (2019).
[30] X. He, M.-B. Hägg, Optimization of carbonization process for preparation of high performance hollow fiber carbon membranes, Ind. Eng. Chem. Res. 50 (13) (2011) 8065–8072.
[31] M. Campo, F. Magalhães, A. Mendes, Carbon molecular sieve membranes from cellophane paper, J. Membr. Sci. 350 (2010) 180–188.
[32] T. Araújo, M. Andrade, G. Bernardo, A. Mendes, Stable cellulose-based carbon molecular sieve membranes with very high selectivities, J. Membr. Sci. 641 (2022), 119852.
[33] L. Lei, A. Lindbråthen, M. Hillestad, M. Sandru, E.P. Favvas, X. He, Screening cellulose spinning parameters for fabrication of novel carbon hollow fiber membranes for gas separation, Ind. Eng. Chem. Res. 58 (29) (2019) 13330–13339.
[34] L. Lei, A. Lindbråthen, M. Sandru, M.T.G. Gutierrez, X. Zhang, M. Hillestad, X. He, Spinning cellulose hollow fibers using 1-Ethyl-3-methylimidazolium Acetate¯Dimethylsulfoxide Co-solvent, Polymers (Basel) 10 (9) (2018) 972.
[35] L. Lei, A. Lindbråthen, X. Zhang, E.P. Favvas, M. Sandru, M. Hillestad, X. He, Preparation of carbon molecular sieve membranes with remarkable CO2/CH4 selectivity for high-pressure natural gas sweetening, J. Membr. Sci. 614 (2020), 118529.
[36] J.W.F. To, J. He, J. Mei, R. Haghpanah, Z. Chen, T. Kurosawa, S. Chen, W.-G. Bae, L. Pan, J.B.H. Tok, J. Wilcox, Z. Bao, Hierarchical N-doped carbon as CO2 adsorbent with high CO2 selectivity from rationally designed polypyrrole precursor, J. Am. Chem. Soc. 138 (3) (2016) 1001–1009.
[37] A. Rehman, S.-J. Park, Tunable nitrogen-doped microporous carbons: delineating the role of optimum pore size for enhanced CO2 adsorption, Chem. Eng. J. 362 (2019) 731–742.
[38] A. Rehman, S.-J. Park, From chitosan to urea-modified carbons: tailoring the ultra-microporosity for enhanced CO2 adsorption, Carbon 159 (2020) 625–637.
[39] C. Pu, J. Zhang, G. Chang, Y. Xiao, X. Ma, J. Wu, T. Luo, K. Huang, S. Ke, J. Li, X. Yang, Nitrogen precursor-mediated construction of N-doped hierarchically porous carbon-supported Pd catalysts with controllable morphology and composition, Carbon 159 (2020) 451–460.
[40] C.L. Rodríguez-Corvera, J.L. Fajardo-Díaz, A.J. Cortés-López, L.E. Jiménez-Ramírez, E. Muñoz-Sandoval, F. López-Urías, Nitrogen-doped carbon fiber sponges by using different nitrogen precursors: synthesis, characterization, and electrochemical activity, Mater. Today Chem. 14 (2019), 100200.
[41] Z. Duan, G. Henkelman, Identification of active sites of pure and nitrogen-doped carbon materials for oxygen reduction reaction using constant-potential calculations, J. Phys. Chem. C 124 (22) (2020) 12016–12023.
[42] E. Sousa, T. Araújo, T. Lagarteira, A. Mendes, H3PO4-activated Phenolic Resin-Derived Carbon Supports for Oxygen Reduction PGM-free Catalysts (P-6FC), VIII Symposium on Hydrogen, Fuel Cells and Advanced Batteries, Buenos Aires, 2022.
[43] R.G. Morais, N. Rey-Raap, J.L. Figueiredo, M.F.R. Pereira, Glucose-derived carbon materials with tailored properties as electrocatalysts for the oxygen reduction reaction, Beilstein J. Nanotechnol. 10 (2019) 1089–1102.
[44] F. Fu, J. Gu, X. Xu, Q. Xiong, Y. Zhang, X. Liu, J. Zhou, Interfacial assembly of ZnO–cellulose nanocomposite films via a solution process: a one-step biomimetic approach and excellent photocatalytic properties, Cellulose 24 (1) (2017) 147–162.
[45] S. Wang, A. Lu, L. Zhang, Recent advances in regenerated cellulose materials, Prog. Polym. Sci. 53 (2016) 169–206.
[46] W. Liu, T. Budtova, P. Navard, Influence of ZnO on the properties of dilute and semi-dilute cellulose-NaOH-water solutions, Cellulose 18 (4) (2011) 911–920.
[47] S. Wang, L. Dong, Z. Li, N. Lin, H. Xu, S. Gao, Sustainable supercapacitors of nitrogen-doping porous carbon based on cellulose nanocrystals and urea, Int. J. Biol. Macromol. 164 (2020) 4095–4103.
[48] C. Dang, Z. Huang, Y. Chen, S. Zhou, X. Feng, G. Chen, F. Dai, H. Qi, Direct dissolution of cellulose in NaOH/Urea/α-Lipoic acid aqueous solution to fabricate all biomass-based nitrogen, sulfur dual-doped hierarchical porous carbon aerogels for supercapacitors, ACS Appl. Mater. Interfaces 12 (19) (2020) 21528–21538.
[49] L. Segal, J.J. Creely, A.E. Martin, C.M. Conrad, An empirical method for estimating the degree of crystallinity of native cellulose using the X-ray diffractometer, Textil. Res. J. 29 (10) (1959) 786–794.
[50] Y. Liu, Y. Nie, F. Pan, L. Zhou, X. Ji, Z. Kang, S. Zhang, Study on ionic liquid/cellulose/coagulator phase diagram and its application in green spinning process, J. Mol. Liq. 289 (2019), 111127.
[51] M.W. Ullah, M. Ul-Islam, S. Khan, Y. Kim, J.K. Park, Structural and physico-mechanical characterization of bio-cellulose produced by a cell-free system, Carbohydr. Polym. 136 (2016) 908–916.
[52] Y.K. Kim, H.B. Park, Y.M. Lee, Preparation and characterization of carbon molecular sieve membranes derived from BTDA–ODA polyimide and their gas separation properties, J. Membr. Sci. 255 (1) (2005) 265–273.
[53] J.C. Santos, F.D. Magalhães, A. Mendes, Contamination of zeolites used in oxygen production by PSA: effects of water and carbon dioxide, Ind. Eng. Chem. Res. 47 (16) (2008) 6197–6203.
[54] A. Gil, P. Grange, Application of the Dubinin-Radushkevich and Dubinin-Astakhov equations in the characterization of microporous solids, Colloids Surf. A Physicochem. Eng. Asp. 113 (1) (1996) 39–50.
[55] M. Andrade, A.J. Parnell, G. Bernardo, A. Mendes, Propane selective carbon adsorbents from phenolic resin precursor, Microporous Mesoporous Mater. 320 (2021), 111071.
[56] D.D. Do, Adsorption Analysis: Equilibria and Kinetics, PUBLISHED BY IMPERIAL COLLEGE PRESS AND DISTRIBUTED BY WORLD SCIENTIFIC PUBLISHING CO, 1998.
[57] C. Nguyen, D.D. Do, Adsorption of supercritical gases in porous media: determination of micropore size distribution, J. Phys. Chem. B 103 (33) (1999) 6900–6908.
[58] C. Nguyen, D.D. Do, K. Haraya, K. Wang, The structural characterization of carbon molecular sieve membrane (CMSM) via gas adsorption, J. Membr. Sci. 220 (1) (2003) 177–182.
[59] S. Fu, G.B. Wenz, E.S. Sanders, S.S. Kulkarni, W. Qiu, C. Ma, W.J. Koros, Effects of pyrolysis conditions on gas separation properties of 6FDA/DETDA:DABA(3:2) derived carbon molecular sieve membranes, J. Membr. Sci. 520 (2016) 699–711.
[60] J. Gong, J. Li, J. Xu, Z. Xiang, L. Mo, Research on cellulose nanocrystals produced from cellulose sources with various polymorphs, RSC Adv. 7 (53) (2017) 33486–33493.
[61] A.D. French, Idealized powder diffraction patterns for cellulose polymorphs, Cellulose 21 (2) (2014) 885–896.
[62] M.a. Fauziyah, W. Widiyastuti, R. Balgis, H. Setyawan, Production of cellulose aerogels from coir fibers via an alkali–urea method for sorption applications, Cellulose 26 (18) (2019) 9583–9598.
[63] R. Li, L. Zhang, M. Xu, Novel regenerated cellulose films prepared by coagulating with water: structure and properties, Carbohydr. Polym. 87 (1) (2012) 95–100.
[64] Y.-T. Lin, J.-Y. Li, H.-H. Tseng, M.-Y. Wey, Insights into the role of polymer conformation on the cutoff size of carbon molecular sieving membranes for hydrogen separation and its novel pore size detection Technology, ACS Appl. Mater. Interfaces 13 (4) (2021) 5165–5175.
[65] D. Saurel, J. Segalini, M. Jauregui, A. Pendashteh, B. Daffos, P. Simon, M. Casas-Cabanas, A SAXS outlook on disordered carbonaceous materials for electrochemical energy storage, Energy Storage Mater. 21 (2019) 162–173.
[66] M. Teubner, R. Strey, Origin of the scattering peak in microemulsions, J. Chem. Phys. 87 (5) (1987) 3195–3200.
[67] V.C. Geiszler, W.J. Koros, Effects of polyimide pyrolysis conditions on carbon molecular sieve membrane properties, Ind. Eng. Chem. Res. 35 (9) (1996) 2999–3003.
[68] K.M. Steel, W.J. Koros, Investigation of porosity of carbon materials and related effects on gas separation properties, Carbon 41 (2) (2003) 253–266.
[69] M. Campo, Carbon Molecular Sieve Membranes for Gas Separation: Study, Preparation and Characterization, University of Porto, Porto, 2009.
[70] Y. Ma, M. Jue, F. Zhang, R. Mathias, H. Jang, R. Lively, Creation of well-defined "mid-sized" micropores in carbon molecular sieve membranes, Angew. Chem. 131 (2019).
[71] Y.-R. Rhim, D. Zhang, D.H. Fairbrother, K.A. Wepasnick, K.J. Livi, R.J. Bodnar, D. C. Nagle, Changes in electrical and microstructural properties of microcrystalline cellulose as function of carbonization temperature, Carbon 48 (4) (2010) 1012–1024.
[72] P.H.T. Ngamou, M.E. Ivanova, O. Guillon, W.A. Meulenberg, High-performance carbon molecular sieve membranes for hydrogen purification and pervaporation dehydration of organic solvents, J. Mater. Chem. 7 (12) (2019) 7082–7091.
[73] J. Zhang, Z. Xia, L. Dai, Carbon-based electrocatalysts for advanced energy conversion and storage, Sci. Adv. 1(7) e1500564.
[74] M. Inagaki, M. Toyoda, Y. Soneda, T. Morishita, Nitrogen-doped carbon materials, Carbon 132 (2018) 104–140.
[75] S.R.M. Santiago, Y.A. Wong, T.-N. Lin, C.-H. Chang, C.-T. Yuan, J.-L. Shen, Effect of nitrogen doping on the photoluminescence intensity of graphene quantum dots, Opt. Lett. 42 (18) (2017) 3642–3645.

[76] T. Kondo, D. Guo, T. Shikano, T. Suzuki, M. Sakurai, S. Okada, J. Nakamura, Observation of Landau levels on nitrogen-doped flat graphite surfaces without external magnetic fields, Sci. Rep. 5 (1) (2015), 16412.
[77] X. Ren, H. Li, J. Chen, L. Wei, A. Modak, H. Yang, Q. Yang, N-doped porous carbons with exceptionally high CO2 selectivity for CO2 capture, Carbon 114 (2017) 473–481.
[78] A.C. Ferrari, J. Robertson, Interpretation of Raman spectra of disordered and amorphous carbon, Phys. Rev. B 61 (20) (2000) 14095–14107.
[79] A. Sadezky, H. Muckenhuber, H. Grothe, R. Niessner, U. Pöschl, Raman microspectroscopy of soot and related carbonaceous materials: spectral analysis and structural information, Carbon 43 (8) (2005) 1731–1742.
[80] J. Gao, W. Yun, H. Wu, X. Liu, L. Wang, Q. Yu, A. Li, H. Wang, C. Song, Z. Gao, M. Peng, Z. Mengtao, N. Ma, J. Wang, W. Zhou, G. Wang, Z. Yin, D. Ma, Construction of sp3/sp2 carbon interface in 3D N-doped nanocarbon for the oxygen reduction reaction, Angew. Chem. 131 (2019).
[81] N.D. Shcherban, P. Mäki-Arvela, A. Aho, S.A. Sergiienko, P.S. Yaremov, K. Eränen, D.Y. Murzin, Melamine-derived graphitic carbon nitride as a new effective metal-free catalyst for Knoevenagel condensation of benzaldehyde with ethylcyanoacetate, Catal. Sci. Technol. 8 (11) (2018) 2928–2937.
[82] S. Haider, A. Lindbråthen, J.A. Lie, M.-B. Hägg, Carbon membranes for oxygen enriched air – Part I: synthesis, performance and preventive regeneration, Separ. Purif. Technol. 204 (2018) 290–297.
[83] S. Haider, A. Lindbrathen, J.A. Lie, M.B. Hagg, Carbon membranes for oxygen enriched air - Part I: synthesis, performance and preventive regeneration, Separ. Purif. Technol. 204 (2018) 290–297.
[84] S. Haider, A. Lindbråthen, J.A. Lie, M.-B. Hägg, Regenerated cellulose based carbon membranes for CO2 separation: durability and aging under miscellaneous environments, J. Ind. Eng. Chem. 70 (2019) 363–371.
[85] X. He, Optimization of deacetylation process for regenerated cellulose hollow fiber membranes, International Journal of Polymer Science 2017 (2017) 8.
[86] S. Haider, A. Lindbrathen, J.A. Lie, M.B. Hagg, Carbon membranes for oxygen enriched air - Part II: techno-economic analysis, Separ. Purif. Technol. 205 (2018) 251–262.